Title
Mapping the Fetomaternal Peripheral Immune System at Term Pregnancy.

Journal
Journal of Immunology, 197(11)

Authors
Fragiadakis, Gabriela
Baca, Quentin
Gherardini, Pier
et al.

Publication Date
2016-12-01

DOI
10.4049/jimmunol.1601195

Peer reviewed

HHS Public Access

Author manuscript

J Immunol. Author manuscript; available in PMC 2017 December 01.

Published in final edited form as:

J Immunol. 2016 December 1; 197(11): 4482–4492. doi:10.4049/jimmunol.1601195.

Mapping the Fetomaternal Peripheral Immune System at Term Pregnancy

Gabriela K. Fragiadakis[*,◊], **Quentin J. Baca**[†,◊], **Pier Federico Gherardini**[*], **Edward A. Ganio**[†], **Dyani K. Gaudilliere**[¶], **Martha Tingle**[†], **Hope L. Lancero**[†], **Leslie S. McNeil**[†], **Matthew H. Spitzer**[*], **Ronald J. Wong**[§], **Gary M. Shaw**[§], **Gary L. Darmstadt**[§], **Karl G. Sylvester**[¶], **Virginia D. Winn**[‡], **Brendan Carvalho**[†], **David B. Lewis**[§,‖], **David K. Stevenson**[§], **Garry P. Nolan**[*], **Nima Aghaeepour**[†,◊], **Martin S. Angst**[†,◊], and **Brice L. Gaudilliere**[†,◊]

[*]Department of Microbiology and Immunology, Stanford University School of Medicine, Stanford, CA 94305-5117

[†]Department of Anesthesiology, Perioperative and Pain Medicine, Stanford University School of Medicine, Stanford, CA 94305-5117

[‡]Department of Obstetrics and Gynecology, Stanford University School of Medicine, Stanford, CA 94305-5117

[§]Department of Pediatrics, Stanford University School of Medicine, Stanford, CA 94305-5117

[¶]Department of Surgery, Stanford University School of Medicine, Stanford, CA 94305-5117

[‖]Division of Allergy, Immunology and Rheumatology, Stanford University School of Medicine, Stanford, CA 94305-5117

Abstract

Preterm labor and infections are the leading causes of neonatal deaths worldwide. During pregnancy, immunological cross talk between the mother and her fetus are critical for the maintenance of pregnancy and the delivery of an immuno-competent neonate. A precise understanding of healthy fetomaternal immunity is the important first step to identifying dysregulated immune mechanisms driving adverse maternal or neonatal outcomes. This study combined single-cell mass cytometry of paired peripheral and umbilical cord blood samples from mothers and their neonates with a graphical approach developed for the visualization of high-dimensional data to provide a high-resolution reference map of the cellular composition and functional organization of the healthy fetal and maternal immune systems at birth. The approach enabled mapping of known phenotypical and functional characteristics of fetal immunity (including the functional hyper-responsiveness of $CD4^+$ and $CD8^+$ T cells and the global blunting of innate immune responses). It also allowed discovery of new properties that distinguish the fetal and maternal immune systems. For example, examination of paired samples revealed differences in endogenous signaling tone that are unique to a mother and her offspring, including increased ERK1/2, MAPKAPK2, rpS6, and CREB phosphorylation in fetal $Tbet^+CD4^+$ T cells, $CD8^+$ T

Address correspondence to: Brice Gaudilliere, Department of Anesthesiology, Perioperative and Pain Medicine, 300 Pasteur Drive, Room S236, Stanford, CA 94305-5117, gbrice@stanford.edu.

[◊]These authors contributed equally

cells, B cells and $CD56^{lo}CD16^{+}$ NK cells and decreased ERK1/2, MAPKAPK2, and STAT1 phosphorylation in fetal intermediate and non-classical monocytes. This highly interactive functional map of healthy fetomaternal immunity builds the core reference for a growing data repository that will allow inferring deviations from normal associated with adverse maternal and neonatal outcomes.

INTRODUCTION

Of the 2.9 million neonatal deaths occurring worldwide each year, the leading causes are preterm birth, infections, and intrapartum-related complications (1,2). Delivery of a healthy term newborn depends on finely tuned innate and adaptive immune mechanisms regulating the balance between fetomaternal tolerance and the development of an immuno-competent fetus. When dysregulated, these mechanisms have been implicated in the pathogenesis of preterm birth and linked to adverse neonatal outcomes, such as neonatal infections and sepsis (3–5). A precise understanding of normal fetomaternal immunity at term gestation is the essential first step to identify immunological deviations associated with pregnancy-related complications.

Contained within distinct but interdependent compartments, umbilical cord and maternal peripheral blood provide uniquely accessible substrates that enable the study of the cellular mechanisms underpinning fetomaternal immunity. Single-cell analyses of cell populations within these immune compartments have substantially advanced our understanding of fetomaternal immune cross talk during pregnancy (5,6). However, the limited parameterization afforded by traditional single-cell technologies has thus far precluded comprehensive representation or mapping of the cellular and functional organization of the fetomaternal immune system. Such standardized mapping would provide an organized and curated dataset of “normal” immunity at term gestation and serve as a critical point of reference to understand deviations from normal that are associated with pathological pregnancies.

The recent development and successful “bedside” application of mass cytometry (also known as Cytometry by Time Of Flight mass spectrometry or CyTOF), a high-dimensional flow cytometry platform, now enables the combined phenotypical and functional characterization of the entire circulating immune system at single-cell resolution (7–12). Novel visualization approaches make possible intuitive exploration of high-dimensional mass cytometry datasets when used in tandem with more traditional quantitative approaches. Scaffold is a graphical approach developed by Spitzer et al., which enables intra- and cross-species comparison of immune cell phenotypes populating different compartments (peripheral blood, spleen, liver, lungs, etc.) and provides a reference onto which immune deviations related to genetic or environmental variations are mapped (13). Here, we apply Scaffold to graphically represent the entire peripheral immune system of mothers and their neonates, in essence taking a snapshot of fetomaternal immunity at term.

Expanding on this analytical framework, we developed a mass cytometry assay to simultaneously examine the phenotype and intracellular signaling activities of all major immune cell subsets derived from fetal umbilical cord and maternal peripheral blood

samples. Three sets of data were obtained from ten mothers and their respective neonates: a first set to describe the distribution of immune cell subsets, a second set to describe the endogenous intracellular signaling activities of immune cell subsets close to the *in vivo* condition; and a third set to quantify the capacity of immune cell subsets to mount a signaling response to an immune challenge. Capacity was inferred by stimulating whole blood samples *ex vivo* with a panel of receptor-specific ligands that engage canonical signaling pathways essential for the differentiation, proliferation, or pathogen response of innate and adaptive immune cells. The major goals of the study were to: 1) construct a high-resolution map of the cellular and functional organization of the fetal and maternal peripheral immune systems at term gestation; and 2) provide a reference of normal fetomaternal immunity for future studies designed to identify deviations associated with pregnancy-related pathologies.

MATERIAL AND METHODS

Study design

Based on the premise that umbilical cord and maternal blood provide a unique immunological window into the fetomaternal peripheral immune system in term pregnancies, a 46-parameter mass cytometry assay was developed to assess the cellular and functional organization of fetal and maternal peripheral immune compartments with single-cell resolution. Studying pairs of mothers and their respective neonates provided a unique opportunity to detect differences that are distinct for each pair. To avoid the effect of stress resulting from active labor on the maternal or fetal immune system, only mothers delivering by scheduled C-section were enrolled.

Subjects

The study was conducted at Lucile Packard Children's Hospital in Stanford, CA. The study was approved by the Institutional Review Board of Stanford University School of Medicine, and all participants gave informed consent. Ten healthy pregnant women scheduled for planned Cesarian (C)-section at term gestation (38.69±1.14 wks gestational age) were enrolled in the study. All C-sections were elective procedures that were scheduled at term gestation. The majority of C-sections (70%) were indicated due to maternal history of a prior C-section with no other fetomaternal pathology. One C-section was scheduled for a history of marginal placenta previa, one for a history of myomectomy and one for suspected macrosomia (weight at birth was 4.1kg). There were no reported pregnancy- or birth-related complications. Maternal demographic characteristics included: age (34.6±4.0 yrs [range: 27–40]); gravidity (3±2); parity (1±1); and maternal BMI (32.1±12.4). Five participants were Caucasian, 3 were Asian, 1 was Hispanic, and 1 reported "other". Neonatal demographics were: 6 males and 4 females with a mean birth weight of 3.50±0.37 kg and Apgar scores at 1 min ranging from 8 to 10.

Sample collection

Maternal peripheral blood was collected by venipuncture prior to C-section into heparinized tubes (sodium heparin, BD Biosciences, San Jose, CA). A dedicated clinical research nurse was present at all deliveries. Prior to C-sections, the obstetrician was instructed to clamp the

umbilical cord at the cut end and at the junction of the cord and placenta to prevent retrograde blood flow into the placenta post-section. Umbilical cord blood was collected from the umbilical vein into a syringe using an 18-ga needle and transferred into the requisite collection tubes within minutes of delivery. Throughout the manuscript we refer to immune cells derived from umbilical cord blood samples as “fetal” immune cells with the understanding that post-C section umbilical cord blood was briefly exposed to different environmental influences than native fetal blood.

Whole blood processing

To ensure comparability between acquired samples, all blood samples were processed using a standardized protocol for stimulation, fixation, storage and processing of whole blood samples for mass cytometry analysis (10–12). To examine the function of fetal and maternal immune cells, whole blood samples were stimulated with a control vehicle to assess endogenous cellular function (unstimulated condition), the Toll-like receptor 4 (TLR4) agonist LPS (LPS condition), or a combination of extracellular cytokines eliciting receptor-specific intracellular responses (interleukin (IL)-2, IL-6, granulocyte macrophage colony-stimulating factor (GM-CSF), and interferon (INF) α2A). The integrity of evoked intracellular responses was assessed at the single-cell level by measuring sentinel signaling events including the phosphorylation (p) of key kinases (p-P38, p-ERK1/2, p-MAPKAPK2, and p-S6K) and transcription factors (p-STAT1, p-STAT3, p-STAT5, p-CREB, and p-NFkB) or total protein levels of regulatory factors (IkB). Stimulation conditions were chosen based on the ability to activate canonical intracellular signaling pathways essential for the differentiation, proliferation, or pathogen response of innate and adaptive immune cells. In the absence of single-cell cytokine expression data (not measured in this study), cytokine stimulations analyzed in combination with expression of specific phenotypic and functional markers were utilized to emphasize aspects of $CD4^+$ T cell differentiation, including Th1 (IFNα2A, Tbet, p-STAT1), Th2 (IL-2, and p-STAT5), Th17 (IL-6 and p-STAT3), and T regulatory cells (Tregs, IL-2, FoxP3, and p-STAT5).

Within 30 min of sample collection, 1.0-mL whole blood aliquots were stimulated with either 1 μg/mL of LPS (E&K Scientific, Santa Clara, CA); a cocktail of 100 ng/mL of IL-2 (BD Biosciences), 100 ng/mL of IL-6 (BD Biosciences), 100 ng/mL of GM-CSF (BD Biosciences), and 100 ng/mL of interferon-α2A (IFNα2A Sigma-Aldrich, St. Louis, MO); or left unstimulated. Samples were incubated at 37°C for 15 min, fixed with a proteomic stabilization buffer (Smart Tube Inc., San Carlos, CA) for 10 min at room temperature, and then frozen at −80°C for storage until further processing. Fixation of whole blood samples before long-time storage – in contrast to freezing and freeze-thawing of live cells – ensures that surface and intracellular epitopes are minimally affected by the freeze-thaw process.

Sample processing and red blood cell lysis

Fixed samples were thawed for 10 min at 4°C and then for 10 min in a water bath kept at room temperature. Samples were then filtered using a 100-μm membrane into a hypotonic lysis solution (Smart Tube Inc.) and incubated for 5 min at room temperature. Samples were centrifuged and re-suspended in lysis solution for 5 min and washed twice with cell-staining media (CSM, PBS with 0.5% BSA, 0.02% NaN_3).

Mass-tag cellular barcoding

To minimize experimental variability, samples were barcoded as previously described (14,15). Briefly, isothiocyanobenzyl-EDTA/Pd (Pd)-based reagents were prepared for mass-tag barcoding. Twenty-well barcode plates were prepared with each well containing a unique combination of 3 Pd isotopes (102, 104, 105, 106, 108, or 110) at a concentration of 200 nM in DMSO. After sample thawing and red blood cell lysis, cells were washed with CSM, then with PBS, and finally with 0.02% saponin in PBS. Barcoding plates were thawed and re-suspended in 1 mL of 0.02% saponin in PBS. Barcoding reagent was added to each sample and each sample was incubated with shaking at room temperature for 15 min. Samples were subsequently washed twice with CSM and pooled into a single tube for antibody staining. Three barcoded plates were utilized to process samples from the entire study. To maximize the sensitivity of the assay for detection of differences unique to fetomaternal pairs, all samples from a fetomaternal pair were barcoded and then stained together, and run simultaneously.

Antibodies

Abs were either obtained pre-conjugated from the manufacturer (Fluidigm, South San Francisco, CA) or were conjugated in-house with the appropriate metal isotopes. Purified unconjugated Abs in protein-free PBS carrier were labeled using the MaxPAR antibody conjugation kit (Fluidigm) according to the manufacturer's instructions. Conjugated Abs were stored at a concentration of 0.2 mg/mL (based on percent yield calculated from measured absorbance at 280 nm) in Candor PBS Antibody Stabilization Solution (Candor Biosciences, Wangen, Germany) at 4°C. All antibodies conjugated in-house as well as those obtained pre-conjugated were titrated and validated on samples that were processed identically to the samples used in the study. Abs were tested for specificity and sensitivity across a range of concentrations (typically, 0.25 to 4 μg/mL) as described in Gaudilliere et al. (10). All but one Ab (GATA3) produced consistent antigen-specific staining above background levels. The anti-GATA3 Ab was thus not utilized in the gating of immune cell subsets included in the analysis. Abs were used at concentrations listed in Supplemental Table 1.

Ab staining

Pooled barcoded samples were incubated with a cocktail of 25 Abs against surface Ag (Supplemental Table 1) for 30 min with shaking at room temperature. Samples were washed with CSM, permeabilized with methanol for 10 min at 4°C, and washed twice with CSM. Samples were subsequently incubated with a cocktail of 13 Abs against intracellular proteins (Supplemental Table 1) for 30 min with shaking at room temperature, and then washed with CSM. Samples were incubated with an iridium intercalator (Fluidigm) with 1.6% PFA in PBS overnight at 4°C.

Mass cytometry

Intercalated samples were washed with once with CSM and twice with double distilled water, and then re-suspended in a solution of normalization beads (Fluidigm). Samples were filtered prior to mass cytometry analysis through a 35-μm membrane and analyzed at a flow

rate of approximately 500 cells/sec. Samples were normalized and de-barcoded as described previously (15,16).

Data analyses

Scaffold maps—Scaffold maps were constructed with minor modifications as described by Spitzer et al. (13). Twenty-eight surface markers and intracellular molecules (phenotypic markers: CD235, CD61, CD45, CD66, CD7, CD19, CD45RA, CD11b, CD4, CD8a, CD11c, CD123, CXCR3, CD161, TCRγδ, CD33, Tbet, FoxP3, CD16, GATA3, CCR9, CD25, CD3, IgM, CD127, HLA-DR, CD14, and CD56) were simultaneously analyzed to phenotype innate and adaptive immune cells using an unsupervised clustering algorithm. Cells were grouped into 100 clusters. The Scaffold map was built by relating derived cell clusters (Fig. 1, gray/red nodes proportionally sized to cell frequency) to manually gated "landmark" cell populations that provided the basic structure of the Scaffold (Fig. 1, black nodes; Supplemental Fig. 1, landmark cell populations highlighted in red). The following populations were used: granulocytes, B cells, $CD4^+$ T cells, $CD8^+$ T cells, NK cells, classical monocytes (cMCs), and classical dendritic cells (cDCs). Graphs were constructed using edge weights based on cosine similarity of the phenotypic expression vectors between clusters and landmarks. A strength of this method is that the distance measured between these nodes can be calculated from data generated from independent experiments allowing for comparability across studies (13). A force-directed algorithm produced a layout indicating phenotypic similarities by the proximity between cell clusters and landmark cell populations. Analyses and visualizations were performed using the Scaffold package in R and the accompanying user interface. Unsupervised clusters were sized proportionally by the frequency of immune cells contained within each cluster. The resulting dataset was uploaded onto an interactive and freely accessible interface (http://52.52.20.124:8080).

Immune feature derivations—CyTOF data from each sample was manually gated into immune cell types of interest (Supplemental Fig. 1) using Cytobank software (Mountain View, CA). The following cell types were included in all analyses: granulocytes, B cells, $CD4^+$ T cells, naïve $CD45RA^+CD4^+$ T cells, memory $CD45RA^-CD4^+$ T cells, $Tbet^+CD4^+$ Th1 cells, Tregs, $CD8^+$ T cells, naïve $CD45RA^+CD8^+$ T cells, memory $CD45RA^-CD8^+$ T cells, γδT cells, $CD56^{hi}CD16^-$ natural killer (NK) cells, $CD56^{lo}CD16^+$ NK cells, cMCs, non-classical monocytes (ncMCs), intermediate monocytes (intMCs), $lin^-CD11b^+CD14^+HLA\text{-}DR^{lo}$ myeloid-derived suppressor cells (MDSCs), cDCs, and plasmacytoid dendritic cells (pDCs). Frequency of immune features was calculated from unstimulated conditions and expressed as a percentage of gated singlets in the case of granulocytes, and as a percentage of mononuclear cells ($CD45^+CD66^-$) in the case of all other cell types.

For signaling immune features (functional immune features), a transformation was applied to the gated data (arcsinh(data/5)). The following signaling proteins or phospho-proteins were used: p-STAT1, p-STAT3, p-STAT5, p-NFkB, IkB, p-MAPKAPK2, p-P38, p-rpS6, p-ERK1/2, and p-CREB. Signaling immune features from unstimulated conditions were calculated as the median transformed value of each signaling protein in each of the gated cell types listed above. Immune signaling features from stimulated conditions (LPS and

cytokines) were calculated by subtracting unstimulated from stimulated transformed data for each patient.

Analyses of significant differences between maternal and neonatal immune features—Differences between maternal and neonatal immune features were assessed using Significance Analysis of Microarrays (SAM) with a false discovery rate (FDR) cutoff of 1% using the same R package (17). In all paired analyses, maternal-neonatal pairs were used. By analogy to the analysis of large genomic dataset, identified signaling immune features were further filtered by applying an effect-size threshold to the absolute value of observed differences, as previously described in Fragiadakis et al. (11). Thresholds were set based on either: 1) a visual breakpoint in the data (cytokine condition, arcsinh ratio > 1.0); or 2) in the absence of a breakpoint, a visual slope change in the data (unstimulated condition, arcsinh ratio > 0.3 and LPS condition, arcsinh ratio > 0.1). A summary of SAM analyses utilized for each dataset is provided in Supplemental Table 2.

Principal component analyses (PCA)—PCA were performed on immune feature data from the 3 signaling conditions (LPS, cytokine, and unstimulated) for each sample (10 neonatal and 10 maternal samples). Samples were plotted based on their values for the first two principal components and subsequently identified as either maternal or neonatal. Calculations were performed in R.

Visualizations and data resources—All plots were created in R primarily using the ggplot2 package. Scaffold maps were created using the scaffold R package user interface. Data is available for download at cytobank.org. Code written to perform this analysis is publically available at github.com/gfragiadakis/neonatals. Interactive Scaffold maps are publicly available online (http://52.52.20.124:8080).

RESULTS

High-resolution organization of the fetomaternal immune landscape

Scaffold maps visualize and contrast the cellular organization of the maternal (Fig. 1A) and fetal (Fig. 1B) immune systems. Navigating across the Scaffold reference map by sequentially coloring cell clusters by phenotypic marker expression revealed striking differences in the organization of the fetal and maternal immune systems, which spanned all hematopoietic compartments. Expected shifts in the fetomaternal distribution of adaptive cells (18–21) (including naïve and memory T-cell subsets, and IgM^+ B cells) were demarcated and visualized alongside noticeable changes in the distribution of innate cell subsets (granulocytes, $CD56^{lo}CD16^+$ NK cells, and $lin^-CD11b^+CD14^+HLA\text{-}DR^{lo}$ MDSCs) (Fig. 1A and Supplemental Fig. 2A–D). Further quantification of the differences visualized on the reference map with a SAM algorithm (17) in 19 manually-gated cells subsets (Supplemental Fig. 1) identified 11 populations (~60% of gated populations) whose frequency differed significantly between the fetal and maternal immune systems (FDR < 0.01).

Results of the SAM analyses of manually gated cell types aligned with the visual examination of the Scaffold reference maps and revealed the phenotypic organization of the

fetomaternal immune landscape (Fig. 1C). Key findings are the proportional increase of naïve relative to memory $CD4^+$ and $CD8^+$ T cells, and the scarcity of $Tbet^+CD4^+$ T cells in the fetal adaptive immune branch (Fig. 1C and Supplemental Fig. 2E), which reflects the relative immaturity of the developing adaptive immune system. It is notable that $Tbet^+CD4^+$ T cells were detectable in fetal cord blood samples, which is reminiscent of recently described populations of memory $CD4^+$Tcells with Th1 function in fetal blood (22). Consistent with this report, in our study fetal immune cells harboring a $CD45RA^-$ memory phenotype were highly represented within the $Tbet^+CD4^+$ T cell compartment (accounting for over 52% of $Tbet^+CD4^+$ T cells, Supplemental Fig. 2F).

Within innate immune compartments, the increased frequency of fetal $CD56^{lo}CD16^+$ NK cells points to the predominant role of the innate immune branch for protecting the neonate against newly encountered pathogens. Interestingly, suppressive innate cells including myeloid derived suppressor cells (MDSCs) were also overrepresented. These cells may be remnants of immuno-tolerant mechanisms established during pregnancy in the intra-uterine environment.

Mapping functional differences in fetal and maternal immune cells at term

We visualized and examined the functional organization of the fetal and maternal immune system by projecting functional attributes (cell signaling activity) onto their respective Scaffold maps depicting the cellular organization. Color-coding the signaling activity of each intracellular marker provided highly accessible qualitative information reflecting the functional state of immune cell clusters across the entire fetal and maternal immune systems (Fig. 2). Functional differences between fetal and maternal immune cell clusters were immediately apparent in large cell clusters representing major immune cell compartments as well as smaller clusters containing rarer cell populations. Examples shown in Figure 2 are the differences in endogenous ERK1/2 signaling activity and evoked STAT1 and P38 signaling in response to *ex vivo* stimulation with cytokines and LPS, respectively. The endogenous p-ERK1/2 signal was strikingly higher in fetal T and B cells compared to those of their respective mothers (Fig. 2A, 2B). The evoked p-STAT1 signal was visibly decreased in fetal monocytes and $CD56^{lo}CD16^+$ NK cells (Fig. 2C, 2D). Finally, the evoked p-P38 signal in granulocytes, monocytes, and cDCs was dramatically decreased in neonates (Fig. 2E, 2F).

Scaffold maps offer a unique platform to visually explore the entire cellular and functional fetomaternal peripheral immune system, and orient us towards differences in abundant as well as scarce innate and adaptive cell populations. These visually compelling findings then prompted further quantitative analyses of the functional differences that distinguish fetal from maternal immune cells. We performed such analyses in a subset of 19 manually gated cell types (Supplemental Fig. 1) that represented the majority of cell clusters revealed by unsupervised clustering analyses rather than all cell clusters in order to reduce the number of comparisons and increase statistical power.

Broad functional differences characterize the fetal and maternal peripheral immune systems

Principal Component Analysis of functional activities measured in each manually gated cell subset at baseline and in response to extracellular stimulations fully separated maternal from fetal blood samples (Fig. 3A). Further characterization of the functional differences between maternal and fetal immune cells using SAM identified 161 significant cell type-specific signaling features out of 570 (Fig. 3B, Supplemental Table 2, FDR < 0.01). Of these signaling features, 18 were statistically significant only when related pairs of fetomaternal samples were examined (Fig. 3B, left, purple circles; SAM paired, FDR < 0.01). Interestingly, all pair-specific differences were endogenous rather than evoked signaling events (Fig, 3C, purple circles). These results emphasize unique differences in the basal signaling "tone" of immune cells from related mother-fetus pairs that would have remained undetected if the dataset had been generated from unrelated populations.

Differences in endogenous signaling activity

Differences in endogenous signaling activity (features) were ranked according to effect size (mean difference between maternal and fetal signal intensities, Fig. 4A). The top 16 features (see Methods) split into 11 features that were elevated (Fig. 4B) and 5 features that were decreased in fetal samples (Fig. 4C). Remarkably, 10 of the 11 elevated features related to signaling activities in adaptive immune cell subsets, including p-ERK1/2, p-MAPKAPK2, p-rpS6, and p-CREB signals in $Tbet^{+}CD4^{+}$ Th1, $CD8^{+}$ T and B cells. Conversely, all of the 5 features that were decreased in fetal samples related to signaling activities in innate immune cells, including p-ERK1/2, p-MAPKAPK2, and p-STAT1 signals in intermediate and non-classical monocytes. The finding that $Tbet^{+}CD4^{+}$ Th1 cells were the only cell type with increased endogenous signaling activities within $CD4^{+}$ T cell compartment prompted a post-hoc analysis of p-ERK1/2, p-MAPKAPK2, p-rpS6, and p-CREB signals in $Tbet^{-}$ naïve and $Tbet^{-}$ memory $CD4^{+}$ T cells. The analysis revealed that endogenous p-ERK1/2, p-MAPKAPK2, p-rpS6 and p-CREB signals were elevated in fetal $Tbet^{-}CD4^{+}$ T cell subsets (FDR < 0.01). However, the magnitude of noted differences between fetal and maternal samples did not pass the significance threshold for effect-size (arcsinh ratio < 0.3, Figure 4A).

These data underscore the functional organization of the fetomaternal immune system at baseline and highlight its polarized structure, which is weighted towards an enhanced adaptive and dampened innate signaling tone of fetal immune cell subsets. While a decreased signaling tone of all innate cells likely reflects the global immaturity of the fetal innate immune system, the increased signaling tone of the adaptive cell types was surprising. This begged the question whether fetal and maternal adaptive cell types also differ in their capacity to mount a functional response when stimulated with an external ligand.

Differences in functional capacity

Differences in signaling responses to *ex vivo* stimulation with a combination of cytokines or LPS were identified with SAM and ranked according to the difference in signal intensities from the control condition (Fig. 5A, 6A).

In response to cytokine stimulation (Fig. 5), 10 immune features (of the top 32 features) were elevated, while 22 were decreased in fetal cells relative to maternal cells (Fig. 5B, 5C). Consistent with endogenous signaling activities, all of the 10 elevated features related to signaling responses in adaptive cell subsets, i.e., p-STAT3 and p-STAT5 in B cells, γδ T cells, and naïve and memory $CD4^+$ and $CD8^+$ T cells. Similarly, the majority (16) of decreased features related to signaling responses in innate immune cells including the p-STAT1 and p-STAT3 signals in $CD56^{lo}CD16^+$ NK cells, granulocytes, cDC and monocyte subsets. The remaining 6 features that were decreased in fetal cells related to signaling responses in adaptive immune cells, i.e., p-STAT1 in naïve and memory $CD4^+$ T cells, naïve $CD8^+$ T cells, γδ T cells, Tregs, and B cells. Given the respective roles of STAT1 and STAT5 in promoting Th1 or Th2 differentiation (23,24), decreased STAT1 and increased STAT5 signaling responses in fetal $CD4^+$ T cells may reflect the diminished capacity of $CD4^+$ T cells to differentiate into functional Th1 cells. More surprising was the finding of signal-specific response patterns (STAT1, STAT3, STAT5) that was shared across fetal adaptive cells of different lineages. This suggests that common mechanisms regulate the activity and differentiation of multiple adaptive cell types of the fetal immune system during the later stage of pregnancy.

In response to LPS stimulation all of the top 22 features were decreased in fetal compared to maternal blood (Fig. 6A, 6B). Specifically, a decrease in p-P38, p-ERK1/2, p-MAPKAPK2, p-rpS6, p-CREB, and p-NFkB signals were observed across multiple innate fetal immune cell subtypes including granulocytes, and monocyte and DC subsets (Fig. 6B). Taken together, the results suggest that signaling events downstream of TLR4, a critical pattern recognition receptor for orchestrating the innate immune response in sterile and infectious inflammation, are broadly blunted across fetal innate immune cells.

Contrasting the fetal and maternal functional immune landscape

The Scaffold reference was used to illustrate the functional balance between the fetal and maternal immune systems across all immune cell subsets (Fig. 6C). Results from the SAM analyses of endogenous and evoked signaling events were mapped on the Scaffold reference (Fig. 6C). Each cell cluster was colored according to the number of signaling features that differed significantly between fetal and maternal samples. The Scaffold map highlights the polarized functional organization of the fetomaternal peripheral immune system, generally characterized by elevated adaptive and diminished innate responsiveness of fetal immune cell subsets. However, there are relevant exceptions to this general pattern as indicated by the p-STAT1 response across all examined adaptive immune cell subsets, which was consistently lower in fetal samples. Our findings thus suggest that while a general pattern characterizes the functional balance between innate and adaptive immune cells at birth, distinct signaling in precisely phenotyped immune cell subsets requires careful examination.

DISCUSSION

This study applied high-dimensional mass cytometry with single-cell resolution to map the cellular and fun pregnancy. Interactive graphical maps (Scaffold) allowed navigating and interrogating the complex dataset with relative ease, and highlighted the global functional

organization of the fetomaternal immune landscape. Scaffold maps and subsequent quantitative analyses revealed marked differences between the neonatal and maternal immune system with respect to the abundance of major immune cell subsets, their functional status, and their capacity to respond to an immune challenge. Thematically, in neonates endogenous signaling activity and functional capacity was broadly dampened across all innate immune cell subsets. A more complex picture emerged for the adaptive immune branch. In adaptive immune cells, differences in endogenous signaling activity and functional capacity were cell type- and signaling pathway-specific (i.e., were either higher or lower across different cell subsets). This likely reflects complex and dynamic adaptations of the developing immune system that are time- and context- sensitive. Importantly, Scaffold maps and data presented here provide the necessary frame onto which future and larger datasets can be superimposed to further define normal fetomaternal immunity and infer deviations from normal that define pregnancy-related pathologies and perinatal complications.

Examining fetal cord blood to study the cellular basis of fetomaternal immunity has been the subject of decades of investigation. Our approach takes advantage of recent technological advances, interactive mapping tools, and novel computational algorithms to map existing and novel knowledge onto a common immune reference. This reference builds on prior efforts characterizing the phenotypic immune cell repertoire in fetal samples by integrating multiple functional dimensions (25,26).

Several themes evolved that extend and resonated with prior work. First, we were able to recapitulate previously reported immune cell distribution characteristics of the neonatal immune system at birth (18–21). These included a preponderance of naïve $CD4^+$ and $CD8^+$ T-cell populations, B cells, NK cells, and MDSCs. With respect to adaptive cell function, our data integrates with established concepts of hyper-responsiveness and Treg-bias of fetal $CD4^+$ T cells (27,28). For instance, STAT5 activity, a hallmark of Treg differentiation (28,29), was higher in fetal naïve $CD4^+$ T than maternal naïve $CD4^+$ T cells in response to IL-2 stimulation. It is remarkable however, that the increased capacity of fetal adaptive immune cells to cytokine stimulation was not restricted to $CD4^+$ T cells, but was also observed in $CD8^+$ T-cell subsets, B cells, and γδ T cells. This novel finding suggests that common mechanisms regulate the activity and differentiation of multiple fetal adaptive cell types during the ultimate phase of gestation. Our results also underscore the global blunting of the innate immune branch in neonates. This is consistent with previous studies examining cord blood leukocytes and documenting the limited capacity of innate immune cells to produce pro-inflammatory cytokines (30,31).

The multiplex analysis of paired fetal and maternal blood samples with mass cytometry enabled intriguing discoveries, particularly with regard to the endogenous signaling tone of the fetomaternal immune system. For example, endogenous p-ERK1/2, p-rpS6, p-MAPKAPK2 and p-CREB signals were increased in fetal $Tbet^+CD4^+$ Th1 cells relative to maternal $Tbet^+CD4^+$ Th1 cells. While increased fetal signaling tone was also observed in $Tbet^-CD4^+$ T cell compartments, differences between fetal and maternal signaling tone were most pronounced in $Tbet^+CD4^+$ Th1 cells. This is a surprising finding given a large body of evidence suggesting that fetal $CD4^+$ T cells have a markedly reduced capacity to

differentiate into Th1 cells under *ex vivo* as well as *in vivo* conditions (18). A possible explanation is that increased endogenous CREB activation impedes Th1 differentiation downstream of Tbet activity. For instance, it has been shown for other cell types that activated CREB can inhibit NFkB's activity (32,33), an important downstream target of Tbet in Tbet-induced th1 differentiation (34–36). The combination of high endogenous signaling tone and blunted functional capacity for acquiring Th1 effector function may in turn promote their differentiation into anergic cells that are unable to carry out immune responses rather than competent effector cells (37). This functional response pattern has previously been reported in fetal $CD4^+$ T cells but also in adults for recent thymic emigrant (RTE) $CD4^+$ T cells (37,38). Thus, observed functional features of fetal $CD4^+$ T cells may reflect, at least in part, a high proportion of RTE T cells generated during the last weeks of pregnancy. These cells may confer immediate protection for the neonate, who will encounter a host of new foreign antigens after delivery. These explanations, which dovetail with recent models of lymphocyte ontogeny of the human fetus (27,28), warrant further exploration.

Our results may also guide future studies investigating the mechanisms driving unique signaling properties of fetal immune cells. For example, we observed shared patterns of transcriptional activation across several adaptive cell populations in response to cytokine stimulation (*e.g.*, the p-STAT1, p-STAT3, and p-STAT5 responses, Fig. 5). This observation suggests that a common mechanism – perhaps an exposure to an intrauterine environmental factor or the impact of rapid expansion of adaptive cell compartments as part of normal fetal growth – may drive these signaling phenotypes in fetal adaptive cell types. Similarly, the blunted signaling response to LPS in multiple fetal innate immune cells (Fig. 6) suggests that a common mechanism inhibits TLR4 signaling in these cell types. For example, the endogenous metabolite adenosine has been shown to inhibit TLR-dependent TNF-α production in fetal classical monocytes (39). It will be interesting to determine whether this endogenous mediator also modulates the TLR4 response of other innate immune cell subtypes that featured a blunted response to a TLR4 ligand in our study.

Our study has limitations. First, enrolled women were a small group of homogeneous patient sample undergoing elective C-section, which may not be representative of the population at large. However, our approach and findings provide the analytical framework and foundational reference dataset that larger studies of fetomaternal immunity can build on and expand by including patients with diverse demographics, different socioeconomic backgrounds, or undergoing normal vaginal delivery. Second, it is difficult to perfectly control for clinical treatments at the time of delivery that may affect the fetal circulating immune system. Exposure of umbilical cord blood to indirect effects of pre-operative antibiotics and neuraxial anesthesia during C-section, as well as the inflammatory and hormonal responses to the surgical intervention are important limitations of using cord blood as a surrogate for fetal blood. However, we reasoned that environmental influences on cord blood immune cells would be minimized in the context of a C-section procedure (average time from incision to delivery of the fetus is 10 to 15 minutes) compared to the relatively long process of labor and normal vaginal delivery of the newborn. Third, the analysis – by design – was performed in blood samples collected at term pregnancy. The dynamic state of the maternal immune system is an important factor to consider when interpreting differences between fetal and maternal immune cells. For instance, properties intrinsic to the developing

fetal immune system may only partially explain the dampened response pattern of fetal innate immune cells to an immune challenge. The pro-inflammatory state and shift towards heightened innate immune responses characteristic of the maternal immune system at term may also contribute to observed differences (40,41). Future experiments mapping maternal immunity throughout and beyond pregnancy will be instrumental in elucidating pregnancy-specific maternal contributions to observed fetomaternal differences. Mapping the healthy non-pregnant adult peripheral immune system onto the current dataset will also provide valuable information regarding the impact of pregnancy on maternal immune profiles. Fourth, neither the set of tested stimulations nor the list of selected surface and intracellular markers was exhaustive. While stimulation conditions were chosen to activate a broad range of canonical immune signaling mechanisms, they were not meant to fully reproduce physiological cellular responses. Expanding the analysis to other stimulation conditions and cellular parameters (including other cytokines, physiological TLR agonists, and T-cell and B-cell receptor ligands) is an exciting prospect that will require input from the entire scientific community.

Term gestation is associated with profound shifts in fetal and maternal immunity driven by cellular mechanisms implicated in the breakdown of fetomaternal tolerance, the onset of labor, and the delivery of an immunocompetent neonate (3). When dysfunctional, these mechanisms reflect and contribute to pregnancy-related pathologies including pre-eclampsia, chorioamnionitis, and preterm labor (4,42). Our efforts are directed towards building a detailed and interactive data repository to characterize the normal cellular and functional organization of the fetal and maternal immune systems. We propose that the construction of such a data repository will yield a reference that will precisely map pathological deviations from normal that are associated with and possibly drive adverse fetal, neonatal, and maternal outcomes.

Supplementary Material

Refer to Web version on PubMed Central for supplementary material.

Acknowledgments

We would like to thank Dr. Elena Hsieh (MD, Departments of Immunology and Microbiology and of Pediatrics, University of Colorado, Children's Hospital Colorado, Denver, CO) for providing guidance in the CyTOF panel design for profiling fetal cord blood. We thank William Magruder and Christine Junge (Department of Anesthesiology, Pain and Perioperative Medicine, Stanford University, Stanford, CA) for critically editing the manuscript.

Source of support: This work was primarily supported by the March of Dimes Prematurity Research Center at Stanford and the Bill and Melinda Gates Foundation (OPP 1017093, OPP1113682); additional funding was provided by the Department of Anesthesiology, Perioperative and Pain Medicine at Stanford University. G.K.F. is supported by the Stanford Bio-X graduate research fellowship (Stanford, CA, USA) and the US National Institutes of Health (T32GM007276; Bethesda, MD, USA). B.G. is supported by the US National Institutes of Health (1K23GM111657-02). The study was also supported in part by the Child Health Research Institute (R.J.W, G.M.S., and D.K.S.), the Mary L. Johnson Research Fund (R.J.W and D.K.S.), the Christopher Hess Research Fund (R.J.W and D.K.S.), the National Institutes of Health 5R01AI10012104 (D.B.L.), U19AI057229 (G.P.N.), 1U19AI100627 (G.P.N.), and the Food and Drug Administration HHSF223201210194C (G.P.N.).

REFERENCES

1. Liu L, Oza S, Hogan D, Perin J, Rudan I, Lawn JE, Cousens S, Mathers C, Black RE. Global, regional, and national causes of child mortality in 2000-13, with projections to inform post-2015 priorities: an updated systematic analysis. Lancet. 2015; 385:430–440. [PubMed: 25280870]
2. UNICEF, W. Levels and trends in child mortality: report 2015. United Nations: The World Bank; New York, USA: UNICEF; 2015. (2015)
3. PrabhuDas M, Bonney E, Caron K, Dey S, Erlebacher A, Fazleabas A, Fisher S, Golos T, Matzuk M, McCune JM, Mor G, Schulz L, Soares M, Spencer T, Strominger J, Way SS, Yoshinaga K. Immune mechanisms at the maternal-fetal interface: perspectives and challenges. Nature immunology. 2015; 16:328–334. [PubMed: 25789673]
4. Romero R, Dey SK, Fisher SJ. Preterm labor: one syndrome, many causes. Science. 2014; 345:760–765. [PubMed: 25124429]
5. Arck PC, Hecher K. Fetomaternal immune cross-talk and its consequences for maternal and offspring's health. Nature medicine. 2013; 19:548–556.
6. Enik Grozdics GT. Antigen Presentation and T Cell Response in Umbilical Cord Blood and Adult Peripheral. Blood Journal of Hematology Research. 2014
7. Bendall SC, Simonds EF, Qiu P, Amir el AD, Krutzik PO, Finck R, Bruggner RV, Melamed R, Trejo A, Ornatsky OI, Balderas RS, Plevritis SK, Sachs K, Pe'er D, Tanner SD, Nolan GP. Single-cell mass cytometry of differential immune and drug responses across a human hematopoietic continuum. Science. 2011; 332:687–696. [PubMed: 21551058]
8. Bandura DR, Baranov VI, Ornatsky OI, Antonov A, Kinach R, Lou X, Pavlov S, Vorobiev S, Dick JE, Tanner SD. Mass cytometry: technique for real time single cell multitarget immunoassay based on inductively coupled plasma time-of-flight mass spectrometry. Analytical chemistry. 2009; 81:6813–6822. [PubMed: 19601617]
9. Bjornson ZB, Nolan GP, Fantl WJ. Single-cell mass cytometry for analysis of immune system functional states. Current opinion in immunology. 2013; 25:484–494. [PubMed: 23999316]
10. Gaudilliere B, Ganio EA, Tingle M, Lancero HL, Fragiadakis GK, Baca QJ, Aghaeepour N, Wong RJ, Quaintance C, El-Sayed YY, Shaw GM, Lewis DB, Stevenson DK, Nolan GP, Angst MS. Implementing Mass Cytometry at the Bedside to Study the Immunological Basis of Human Diseases: Distinctive Immune Features in Patients with a History of Term or Preterm Birth. Cytometry. Part A : the journal of the International Society for Analytical Cytology. 2015; 87:817–829. [PubMed: 26190063]
11. Fragiadakis GK, Gaudilliere B, Ganio EA, Aghaeepour N, Tingle M, Nolan GP, Angst MS. Patient-specific Immune States before Surgery Are Strong Correlates of Surgical Recovery. Anesthesiology. 2015; 123:1241–1255. [PubMed: 26655308]
12. Gaudilliere B, Fragiadakis GK, Bruggner RV, Nicolau M, Finck R, Tingle M, Silva J, Ganio EA, Yeh CG, Maloney WJ, Huddleston JI, Goodman SB, Davis MM, Bendall SC, Fantl WJ, Angst MS, Nolan GP. Clinical recovery from surgery correlates with single-cell immune signatures. Science translational medicine. 2014; 6:255ra131.
13. Spitzer MH, Gherardini PF, Fragiadakis GK, Bhattacharya N, Yuan RT, Hotson AN, Finck R, Carmi Y, Zunder ER, Fantl WJ, Bendall SC, Engleman EG, Nolan GP. IMMUNOLOGY. An interactive reference framework for modeling a dynamic immune system. Science. 2015; 349:1259425. [PubMed: 26160952]
14. Behbehani GK, Thom C, Zunder ER, Finck R, Gaudilliere B, Fragiadakis GK, Fantl WJ, Nolan GP. Transient partial permeabilization with saponin enables cellular barcoding prior to surface marker staining. Cytometry. Part A : the journal of the International Society for Analytical Cytology. 2014
15. Zunder ER, Finck R, Behbehani GK, Amir el AD, Krishnaswamy S, Gonzalez VD, Lorang CG, Bjornson Z, Spitzer MH, Bodenmiller B, Fantl WJ, Pe'er D, Nolan GP. Palladium-based mass tag cell barcoding with a doublet-filtering scheme and single-cell deconvolution algorithm. Nature protocols. 2015; 10:316–333. [PubMed: 25612231]

16. Finck R, Simonds EF, Jager A, Krishnaswamy S, Sachs K, Fantl W, Pe'er D, Nolan GP, Bendall SC. Normalization of mass cytometry data with bead standards. Cytometry. Part A : the journal of the International Society for Analytical Cytology. 2013; 83:483–494. [PubMed: 23512433]
17. Tusher VG, Tibshirani R, Chu G. Significance analysis of microarrays applied to the ionizing radiation response. Proceedings of the National Academy of Sciences of the United States of America. 2001; 98:5116–5121. [PubMed: 11309499]
18. Hong, DK.; L, D. Infectious Disease of the Fetus and Newborn Infant. eigth. Wilson, CB.; Nizet, V.; Klein, JO.; Maldonado, Y.; Remington, JS., editors. Philadelphia: Elsevier Saunders; 2014. p. 81-188.
19. Basford C, Forraz N, McGuckin C. Optimized multiparametric immunophenotyping of umbilical cord blood cells by flow cytometry. Nature protocols. 2010; 5:1337–1346. [PubMed: 20595961]
20. Chirumbolo S, Ortolani R, Veneri D, Raffaelli R, Peroni D, Pigozzi R, Colombatti M, Vella A. Lymphocyte phenotypic subsets in umbilical cord blood compared to peripheral blood from related mothers. Cytometry. Part B, Clinical cytometry. 2011; 80:248–253.
21. Gervassi A, Lejarcegui N, Dross S, Jacobson A, Itaya G, Kidzeru E, Gantt S, Jaspan H, Horton H. Myeloid derived suppressor cells are present at high frequency in neonates and suppress in vitro T cell responses. PloS one. 2014; 9:e107816. [PubMed: 25248150]
22. Zhang X, Mozeleski B, Lemoine S, Deriaud E, Lim A, Zhivaki D, Azria E, Le Ray C, Roguet G, Launay O, Vanet A, Leclerc C, Lo-Man R. CD4 T cells with effector memory phenotype and function develop in the sterile environment of the fetus. Science translational medicine. 2014; 6:238–272.
23. Afkarian M, Sedy JR, Yang J, Jacobson NG, Cereb N, Yang SY, Murphy TL, Murphy KM. T-bet is a STAT1-induced regulator of IL-12R expression in naive CD4+ T cells. Nature immunology. 2002; 3:549–557. [PubMed: 12006974]
24. Zhu J, Cote-Sierra J, Guo L, Paul WE. Stat5 activation plays a critical role in Th2 differentiation. Immunity. 2003; 19:739–748. [PubMed: 14614860]
25. Strauss-Albee DM, Fukuyama J, Liang EC, Yao Y, Jarrell JA, Drake AL, Kinuthia J, Montgomery RR, John-Stewart G, Holmes S, Blish CA. Human NK cell repertoire diversity reflects immune experience and correlates with viral susceptibility. Science translational medicine. 2015; 7:297–115.
26. Ornatsky O, Bandura D, Baranov V, Nitz M, Winnik MA, Tanner S. Highly multiparametric analysis by mass cytometry. Journal of immunological methods. 2010; 361:1–20. [PubMed: 20655312]
27. Mold JE, Venkatasubrahmanyam S, Burt TD, Michaelsson J, Rivera JM, Galkina SA, Weinberg K, Stoddart CA, McCune JM. Fetal and adult hematopoietic stem cells give rise to distinct T cell lineages in humans. Science. 2010; 330:1695–1699. [PubMed: 21164017]
28. Mold JE, McCune JM. Immunological tolerance during fetal development: from mouse to man. Advances in immunology. 2012; 115:73–111. [PubMed: 22608256]
29. Cohen AC, Nadeau KC, Tu W, Hwa V, Dionis K, Bezrodnik L, Teper A, Gaillard M, Heinrich J, Krensky AM, Rosenfeld RG, Lewis DB. Cutting edge: Decreased accumulation and regulatory function of CD4+ CD25(high) T cells in human STAT5b deficiency. J Immunol. 2006; 177:2770–2774. [PubMed: 16920911]
30. De Wit D, Olislagers V, Goriely S, Vermeulen F, Wagner H, Goldman M, Willems F. Blood plasmacytoid dendritic cell responses to CpG oligodeoxynucleotides are impaired in human newborns. Blood. 2004; 103:1030–1032. [PubMed: 14504106]
31. De Wit D, Tonon S, Olislagers V, Goriely S, Boutriaux M, Goldman M, Willems F. Impaired responses to toll-like receptor 4 and toll-like receptor 3 ligands in human cord blood. Journal of autoimmunity. 2003; 21:277–281. [PubMed: 14599853]
32. Wen AY, Sakamoto KM, Miller LS. The role of the transcription factor CREB in immune function. J Immunol. 2010; 185:6413–6419. [PubMed: 21084670]
33. Parry GC, Mackman N. Role of cyclic AMP response element-binding protein in cyclic AMP inhibition of NF-kappaB-mediated transcription. J Immunol. 1997; 159:5450–5456. [PubMed: 9548485]

34. Oh H, Ghosh S. NF-kappaB: roles and regulation in different CD4(+) T-cell subsets. Immunological reviews. 2013; 252:41–51. [PubMed: 23405894]
35. Hilliard BA, Mason N, Xu L, Sun J, Lamhamedi-Cherradi SE, Liou HC, Hunter C, Chen YH. Critical roles of c-Rel in autoimmune inflammation and helper T cell differentiation. The Journal of clinical investigation. 2002; 110:843–850. [PubMed: 12235116]
36. Aronica MA, Mora AL, Mitchell DB, Finn PW, Johnson JE, Sheller JR, Boothby MR. Preferential role for NF-kappa B/Rel signaling in the type 1 but not type 2 T cell-dependent immune response in vivo. J Immunol. 1999; 163:5116–5124. [PubMed: 10528218]
37. Palin AC, Ramachandran V, Acharya S, Lewis DB. Human neonatal naive CD4+ T cells have enhanced activation-dependent signaling regulated by the microRNA miR-181a. J Immunol. 2013; 190:2682–2691. [PubMed: 23408835]
38. Haines CJ, Giffon TD, Lu LS, Lu X, Tessier-Lavigne M, Ross DT, Lewis DB. Human CD4+ T cell recent thymic emigrants are identified by protein tyrosine kinase 7 and have reduced immune function. The Journal of experimental medicine. 2009; 206:275–285. [PubMed: 19171767]
39. Levy O, Coughlin M, Cronstein BN, Roy RM, Desai A, Wessels MR. The adenosine system selectively inhibits TLR-mediated TNF-alpha production in the human newborn. J Immunol. 2006; 177:1956–1966. [PubMed: 16849509]
40. Kraus TA, Engel SM, Sperling RS, Kellerman L, Lo Y, Wallenstein S, Escribese MM, Garrido JL, Singh T, Loubeau M, Moran TM. Characterizing the pregnancy immune phenotype: results of the viral immunity and pregnancy (VIP) study. Journal of clinical immunology. 2012; 32:300–311. [PubMed: 22198680]
41. Kraus TA, Sperling RS, Engel SM, Lo Y, Kellerman L, Singh T, Loubeau M, Ge Y, Garrido JL, Rodriguez-Garcia M, Moran TM. Peripheral blood cytokine profiling during pregnancy and post-partum periods. American journal of reproductive immunology. 2010; 64:411–426. [PubMed: 20712812]
42. Kan B, Razzaghian HR, Lavoie PM. An Immunological Perspective on Neonatal Sepsis. Trends in molecular medicine. 2016; 22:290–302. [PubMed: 26993220]

Abbreviations used in this article

IFNα2A	interferon-α2A
cMCs	classical monocytes
cDCs	classical dendritic cells
MDSC	myeloid-derived suppressor cell
NK	nature killer
pDCs	plasmacytoid dendritic cells
SAM	Significance Analysis of Microarrays
FDR	false discovery rate
PCA	principal component analyses
Tregs	regulatory T cells
RTE	recent thymic emigrant
p−	phosphorylated
CREB	cAMP response element-binding protein

STAT	Signal transducer and activator of transcription
NF-kB	nuclear factor kappa-light-chain-enhancer of activated B cells
IkB	NF-kB inhibitor alpha
MAPK	Mitogen-activated protein kinases
MAPKAPK2	MAPK activated protein kinase 2
rp-S6	ribosomal protein-S6
Tbet	T box transcription factor
FOXP3	forkhead box P3
ERK1/2	extracellular signal–regulated kinase 1/2.

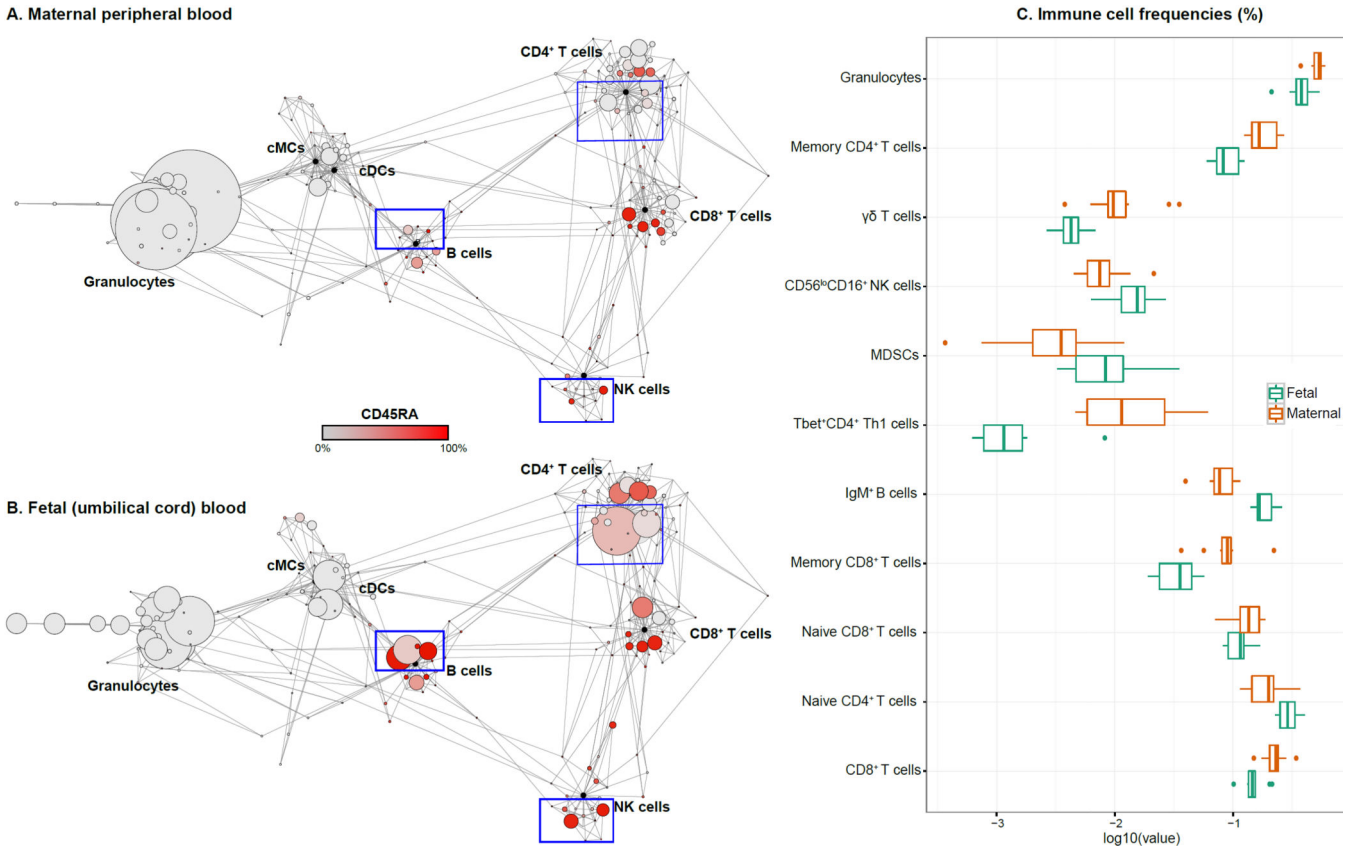

FIGURE 1. Scaffold maps provide a reference for the cellular organization of the normal fetal and maternal peripheral immune systems at term gestation

Scaffold maps of immune cells in maternal peripheral (**A**) and fetal cord (**B**) blood. A representative example from pairs of maternal and fetal samples is shown. Black nodes denote landmark cell populations that define the basic structure of the Scaffold map (i.e., manually-gated granulocytes, Gr; classical monocytes, cMCs; classical dendritic cells, cDCs; natural killer cells, NK cells; B cells; and $CD4^+$ and $CD8^+$ T cells, Supplemental Fig. 1). Landmark populations are the critical anchors for organizing cell clusters derived from unsupervised clustering analyses. Cell clusters are connected to landmark populations of similar phenotypes and are sized based on the frequency of cells contained in each cluster. In this example, the color scale (grey to red) varies proportionally to the median CD45RA expression of cells contained within each cluster. Rectangles highlight noticeable neonatal-maternal differences for naïve $CD4^+$ T cells ($CD45RA^+$ cells), IgM^+ B cells, and $CD56^{lo}CD16^+$ NK cells (see also Supplemental Fig. 2A–D). (**C**) Statistically significant differences in immune cell frequencies between maternal and fetal samples. The analyses comprised 19 manually gated cell populations (see gating hierarchy, Supplemental Fig. 1) that represented the majority of displayed cell clusters (FDR < 0.01, SAM two-class paired, n = 20). Cell populations that differed significantly are plotted on a log10 scale. The relative distribution of naïve and memory $CD4^+$ and $CD8^+$ T-cell subsets were further quantified as a percentage of total $CD4^+$ and $CD8^+$ T cells and highlighted the preponderance of naïve T cells in fetal compared to maternal samples (Supplemental Fig. 2E).

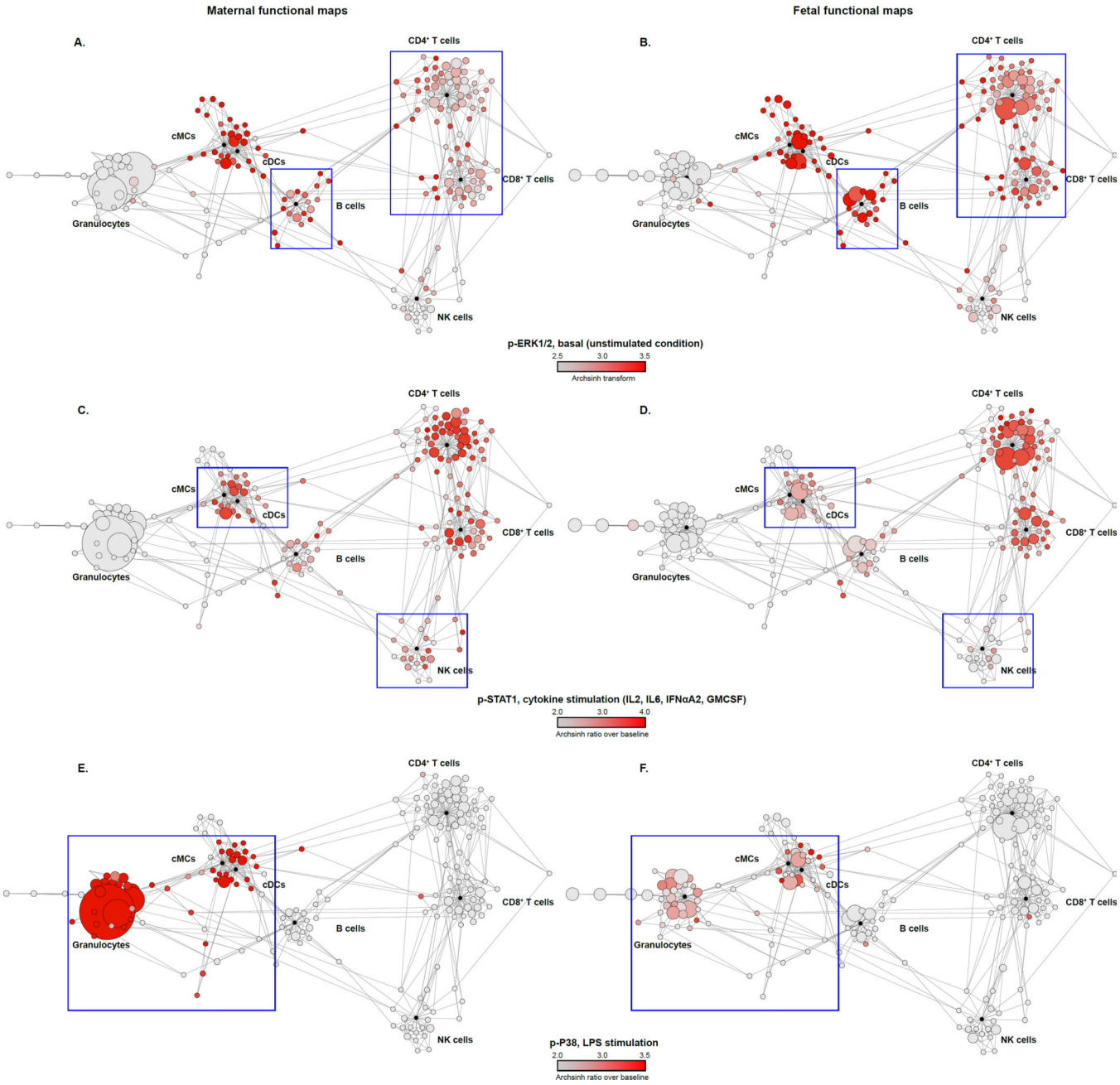

FIGURE 2. Scaffold maps provide a reference for the functional organization of the normal fetal and maternal peripheral immune systems at term gestation

Scaffold maps of immune cell functions in maternal peripheral (**A, C, E**) and fetal cord (**B, D, F**) blood samples. Representative examples from one pair of maternal and fetal samples are shown. Individual cell clusters are colored based on indicated intracellular signaling activities. Median endogenous p-ERK1/2 signal (Arcsinh transform) in unstimulated maternal (**A**) and fetal (**B**) samples. Increased fetal p-ERK1/2 signaling in clusters within the $CD4^+$ T, $CD8^+$ T, and B cell landmark populations is highlighted in blue rectangles. Median p-STAT1 signaling response to cytokine stimulation with IL-2, IL-6, GM-CSF, and IFNα2A in maternal (**C**) and fetal (**D**) samples. Decreased fetal p-STAT1 signaling response in

clusters within the classical monocyte (cMC), classical dendritic cell (cDC), and natural killer (NK) cell landmark populations is highlighted in blue rectangles. Median p-P38 signaling response to TLR4 stimulation with LPS. Decreased fetal p-P38 signaling response in clusters within the cMC, cDC, and granulocyte landmark cell populations in maternal (**E**) and fetal (**F**) samples are highlighted in blue rectangles.

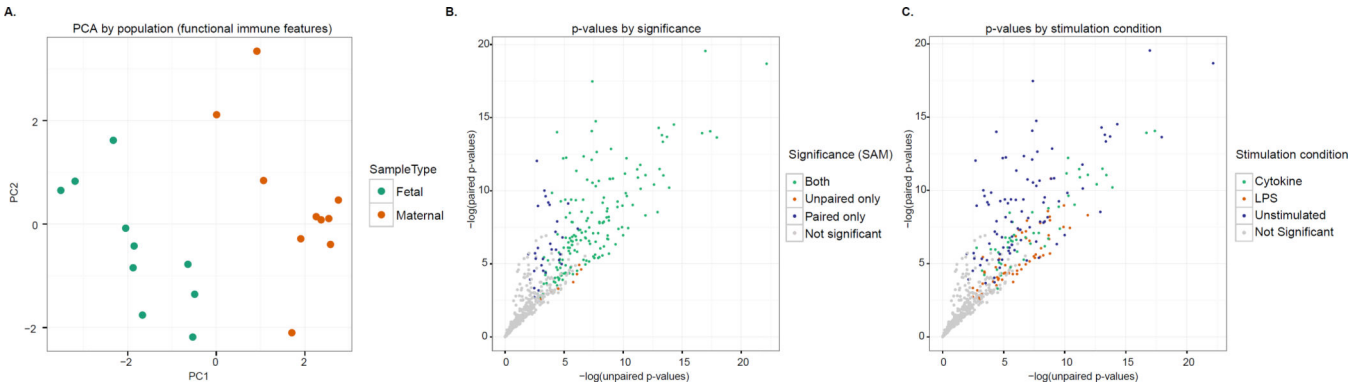

FIGURE 3. Paired analysis of related maternal and fetal samples enables detection of unique pair-specific differences in endogenous signaling activity

(**A**) Principal component analysis (PCA) perfectly separated signaling activities (functional immune features; total of 570 per subject) in fetal and maternal immune cells. Dot plots represent values along the first PC-axis for neonatal cord blood (teal circles) or maternal blood samples (orange circles). (**B, C**) Dot plots represent *p*-values for fetal-maternal differences between functional immune features when incorporating paired information (paired t-test, *y-axis*) or excluding paired information (unpaired t-test, *x-axis*). In (**B**), colors indicate whether signaling features were statistically significant when using a paired analysis only (purple circles, SAM two-class paired), an unpaired analysis only (orange circles, SAM two-class unpaired), or both, i.e., a paired and unpaired analysis (teal circles). In (**C**), colors indicate stimulation conditions. All features that were significant only in a paired analysis corresponded to *endogenous* signaling activities, i.e., the signaling tone of immune cell subsets close to the *in vivo* condition.

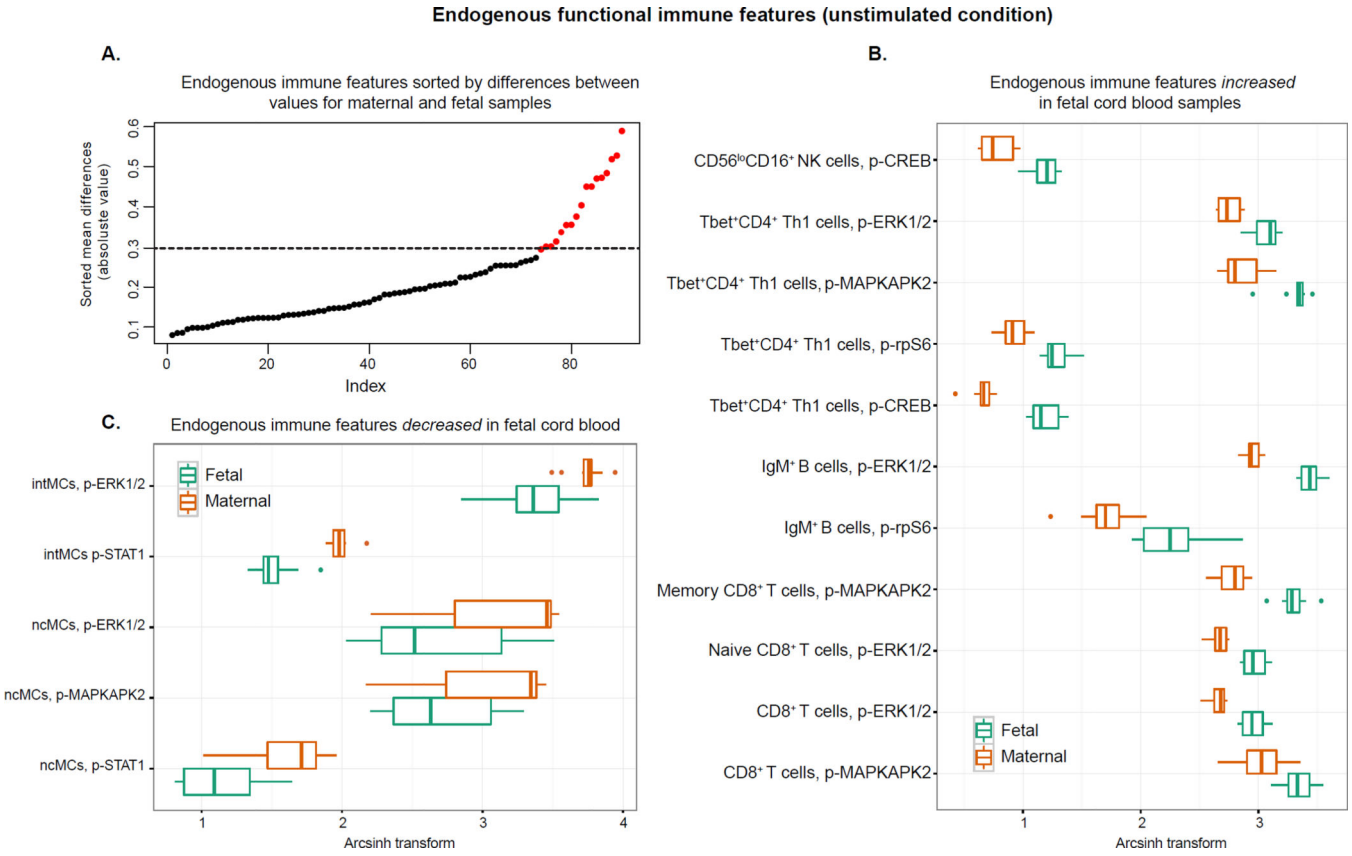

FIGURE 4. Endogenous signaling activity of fetal and maternal immune cells at term gestation

(**A**) Significant endogenous immune features ordered by effect size (mean difference between values in paired maternal and fetal samples, FDR < 0.01, SAM two-class paired). Dashed line indicates noticeable change in slope of the ranked FDR values, which separates the 16 most significant immune features (red circles) from all other significant immune features. These 16 immune features are plotted in panels (**B**) (higher in fetal than in maternal samples) and (**C**) (higher in maternal than in fetal samples). All features that were higher in maternal samples were identified in innate immune cell subsets, while 10 out of 11 features that were higher in fetal samples were identified in adaptive immune cell subsets.

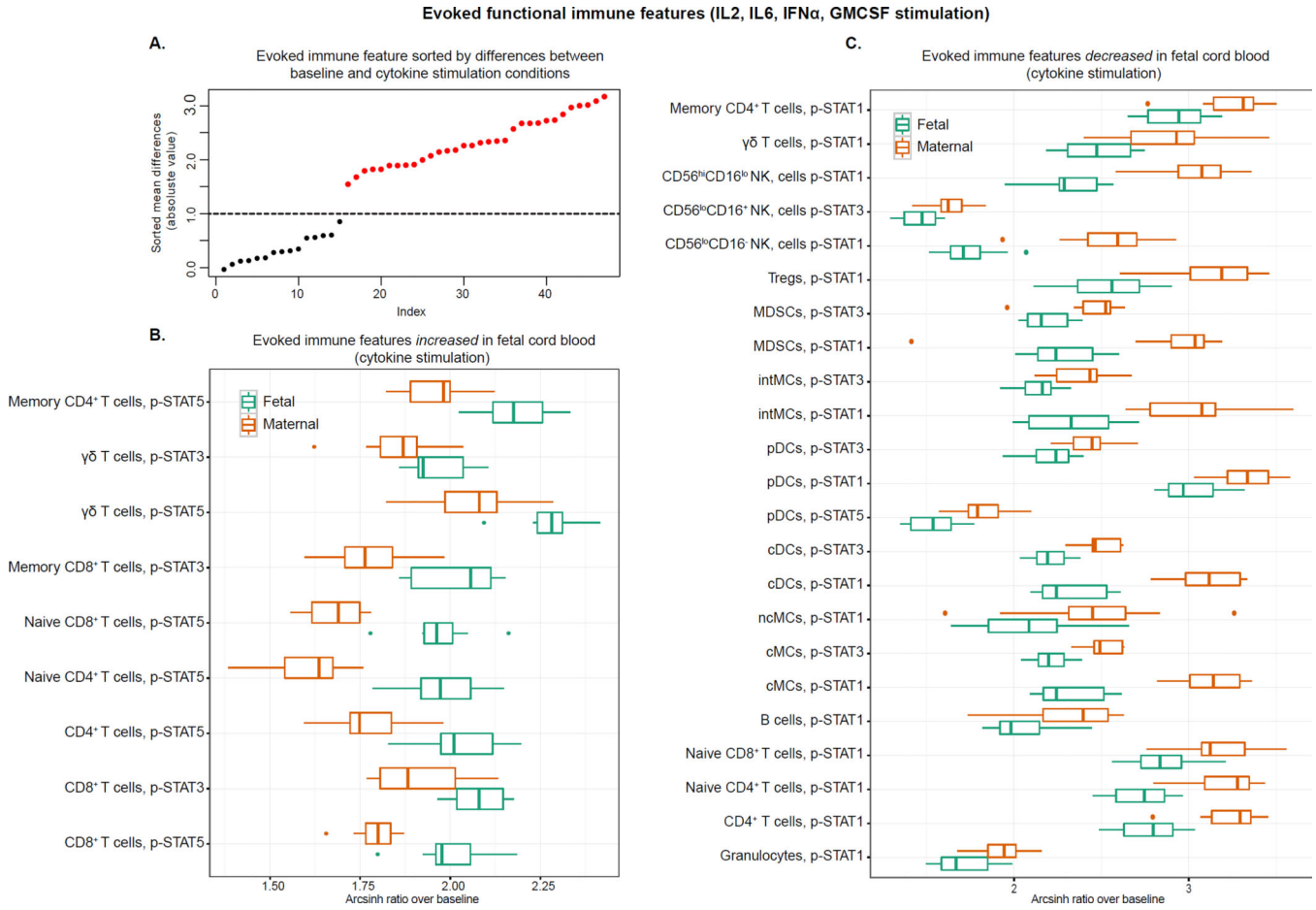

FIGURE 5. Signaling activity of fetal and maternal immune cells in response to cytokine stimulation (IL-2, IL-6, IFNα2A, and GM-CSF)

(**A**) Significant “evoked immune features” ordered by effect size (mean signal induction from unstimulated condition, FDR < 0.01, SAM two-class paired). The dashed line indicates change in the slope of the ranked data. The 32 most significant evoked immune features are shown in red. (**B**) Evoked immune features that are higher in fetal samples are shown. (**C**) Evoked immune features that are lower in fetal samples are shown. About 70% of evoked immune features that were lower in fetal samples are identified in innate immune cell subsets, while 100% of evoked immune features that were higher are identified in adaptive immune cells.

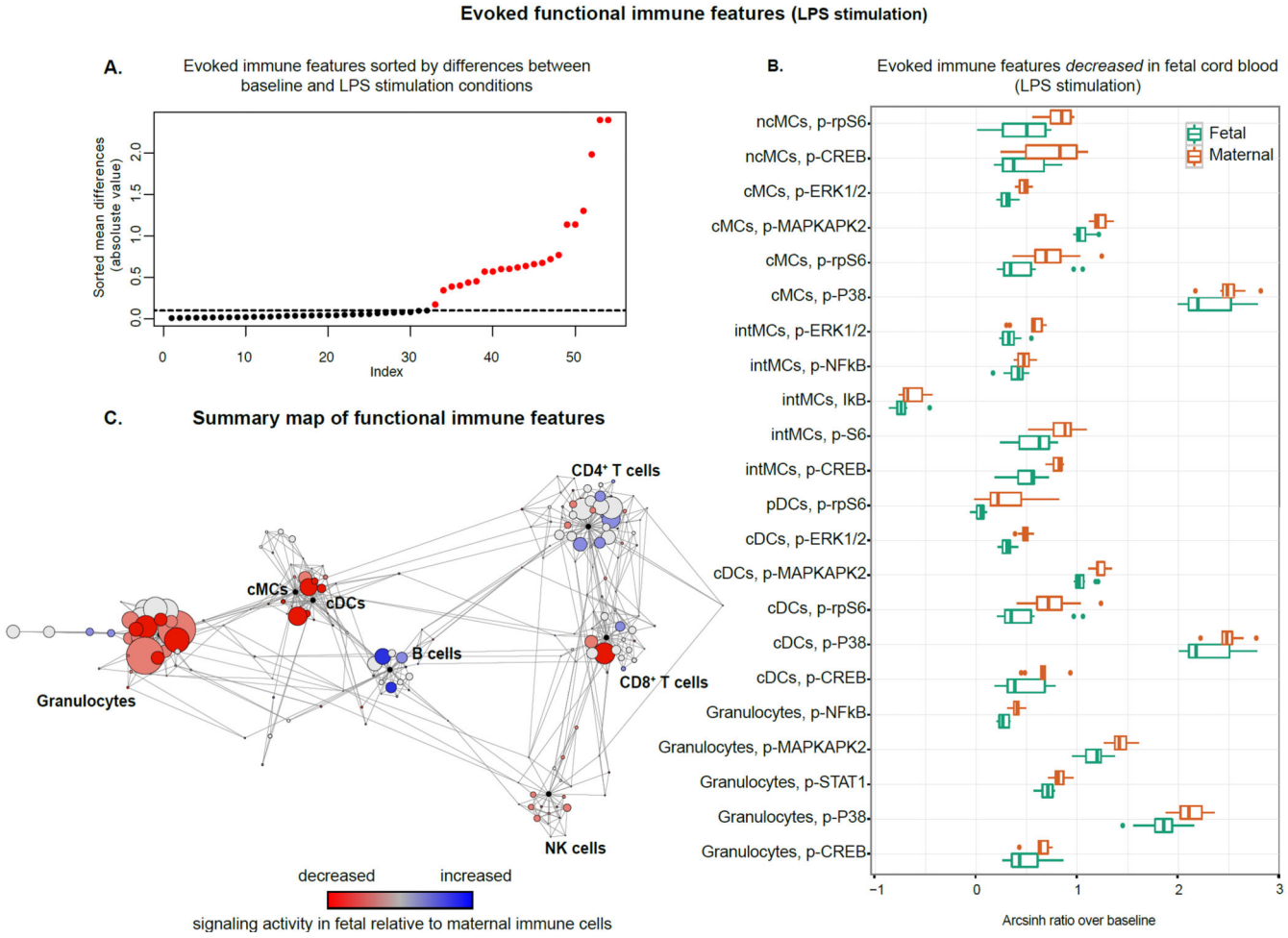

FIGURE 6. Signaling activity of fetal and maternal immune cells in response to TLR4 agonist (LPS)

(**A**) Significant evoked immune features in response to LPS stimulation ordered by effect size (mean signal induction from unstimulated condition, FDR < 0.01, SAM two-class paired). The dashed line indicates change in the slope of ranked data. The 22 most significant evoked immune features (red circles) are plotted in panel (**B**). All significant evoked immune features were lower in the neonatal samples. (**C**) Scaffold map summarizing all functional immune features that differed significantly between fetal and maternal immune cells (endogenous and LPS and cytokine stimulations). Immune cell clusters containing functional immune features characterized by decreased signaling activity in maternal cell clusters relative to fetal cell clusters are shown as blue circles, while increased signaling activity in maternal cell clusters relative to fetal cell clusters are shown as red circles.